Benzocarbazole anions intercalated layered double hydroxide and its tunable fluorescence†

Dongpeng Yan,[a] **Jun Lu,**[*a] **Jing Ma,**[b] **Min Wei,**[*a] **David G. Evans**[a] **and Xue Duan**[a]

Luminescent benzocarbazole anions (BCZC) intercalated into the interlayer region of Mg–Al-layered double hydroxides (BCZC/LDH) with different layered charge densities (LCD) were prepared. The structure and chemical composition of the composites were characterized by X-ray diffraction, elemental analysis, thermogravimetry and differential thermal analysis (TG-DTA), infrared spectra (FT-IR), UV-vis absorption and fluorescence spectroscopy. The photoemission behavior of BCZC in the LDH matrix with high (Mg/Al ratio = 1.801) and low (Mg/Al ratio = 3.132) LCD is similar to that of BCZC solid and aqueous solution states respectively, indicating that the luminescence performances of the intercalated dye anions can be tuned by adjusting the LCD of the LDH layer. Moreover, the thermal stability and stacking order of BCZC are largely improved upon intercalation, and the BCZC/LDH thin film exhibits well polarized luminescence with the luminescent anisotropy of 0.15–0.20. In addition, molecular dynamics (MD) simulation was employed to calculate the basal spacing and molecular arrangement of the intercalated BCZC within the LDH matrix. The simulation results show that the distribution of BCZC anions is much broader in the gallery of Mg–Al-LDH with high LCD, while BCZC anions exhibit a more ordered arrangement in LDH with low LCD. Furthermore, the radial distribution functions of interlayer water molecules were also studied. Based on the combination of experiment and theoretical simulation, this work provides a detailed understanding of the tunable photoluminescence, orientation and diffusion behavior of the luminescent molecules confined within the gallery of a 2D inorganic matrix.

1. Introduction

Organic fluorescence dye materials have drawn much attention due to their potential applications in the field of solid state self-emission devices.[1] Generally, these dye molecules have the advantages of easy processing, simple structure, low cost and high quantum yield, facilitating the fabrication of well-defined luminescent thin-film materials. However, dye-type luminescent materials are prone to aggregate formation in the solid state, resulting in red-shift of fluorescence, broadening and even quenching. This is unfavorable for the high luminescent efficiency of dye molecules. Moreover, the relatively poor thermal or optical stability should be improved when applying these materials into optoelectronic applications. One attractive and effective solution to these problems is the incorporation of dye molecules into solid host matrices, since the homogeneous distribution of dye molecules in solid matrices at the molecular level can be achieved, which would inhibit the dye aggregation

and thus avoid fluorescence quenching effectively. Moreover, the solid matrices can offer a stable and robust environment to meet the need for the improvement of mechanical, thermal and photostability of dye molecules.

One family of solid matrices fulfilling these criteria is layered double hydroxides (LDHs), which can be described by the general formula: $[M^{II}_{1-x}M^{III}_x(OH)_2]^{z+}A^{n-}_{z/n}\cdot yH_2O$, where M^{II} and M^{III} are divalent and trivalent metals ions, respectively, and A^{n-} is an anion. The structure of the LDH layer is analogous to that of brucite with edge-sharing $M(OH)_6$ octahedra, in which partial substitution of M^{3+} cations for M^{2+} cations induces positively-charged host layers, balanced by the interlayer anions. Recently, LDHs have received much attention from both chemical industry and academia for their potential applications in the fields of catalysis,[2] separation processes[3] and drug delivery.[4] Moreover, some luminescent dye molecules, such as fluorescein,[5a] rhodamine B,[5b] pyrene derivatives,[5c,d] perylene chromophores,[5e] π-conjugated polymers[5f,g] and photoactive complexes[5h] have also been intercalated into LDHs to achieve superior optical performances and luminescent efficiency. In addition, the immobilization of dye in the LDH matrix can reduce environmental pollution or operational risks, which is favorable for their application in solid-state optoelectronic devices.[6] Last but not least, it can be expected that the luminescent properties of dye molecules can be tuned by rationally changing the LDH host structure (such as layered charge density), the orientation and alignment of the dye species, and the host–guest interactions (such as the electrostatic and van der Waals interactions).

[a] *State Key Laboratory of Chemical Resource Engineering, Beijing University of Chemical Technology, Beijing 100029, P. R. China. E-mail: lujun@mail.buct.edu.cn, weimin@mail.buct.edu.cn; Fax: +86-10-64425385; Tel: +86-1064412131*
[b] *School of Chemistry and Chemical Engineering, Key Laboratory of Mesoscopic Chemistry of MOE, Nanjing University, Nanjing 210093, P. R. China*

† Electronic supplementary information (ESI) available: Mean square displacements as a function of simulation time for the BCZC anions in LDH gallery; the radial distribution function of the confined water molecules. See DOI: 10.1039/c0cp00854k

Recently, owing to the limitation of the experimental approaches, the molecular dynamic (MD) simulation method has become an essential technique to study and predict the structures and properties of functional materials, which largely extends the scope of investigation and exploration beyond experiment. The MD simulation method has been employed to study organic and inorganic anion intercalated LDH systems,[7] which demonstrates its feasibility in investigating both structural and functional properties of LDH-based composite materials.[7a] The hydration energy, swelling behavior, radial distribution functions (RDFs) and self-diffusion properties of guests were firstly reported by Newman et al.[7b] The arrangement and geometry of anions within the LDH gallery, such as inorganic anions (CO_3^{2-}, Cl^-),[7f–h] drug anions (ibuprofen)[7i] and biological macromolecules (DNA),[7j] were also probed. However, very few attempts were focused on the correlation between orientation/aggregation of guests and layered charge densities (LCD) of LDH, which would give further insight for the understanding of host–guest interactions as well as obtaining composite materials with superior functionalities.

Carbazole dye is one kind of important luminescent material with excellent performance. Carbazole and its derivatives belong to a large π-conjugated system and exhibit strong intramolecular electron transfer ability, and they have been studied, developed and applied as good optical materials. To the best of our knowledge, however, the research regarding incorporation of carbazole or its derivatives into the inter-gallery of LDHs has never been reported. In this work, the thermal stability and spectroscopic properties of one carbazole derivative (2-hydroxy benzo[a]carbazole-3-carboxylate, denoted as BCZC, shown in Scheme 1) intercalated LDH were studied by thermogravimetric and differential thermal analysis (TG-DTA), FT-IR, UV-vis absorption and fluorescence spectroscopy. It was found that the photoemission behavior of BCZC is dependent on the layered charged density of LDH, and BCZC/LDH thin films exhibit well-defined polarized photoemission anisotropy. Moreover, MD simulation was performed by employing a modified version of the cff91 forcefield[7f,m,n] to analyze the orientation and aggregation of the confined BCZC molecules. The simulation results of the basal spacing and ordered degree are in reasonable agreement with the experimental results, demonstrating the feasibility of MD simulation for this dye/LDH system. Therefore, this work provides a feasible methodology of combining experimental technologies and theoretical simulations for the purpose of understanding the structure and the arrangement of guest species confined in a LDH matrix. It is anticipated that the photoluminescent composites in this work can be potentially used in the field of polarized materials.
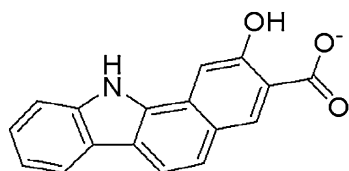
Scheme 1 The chemical structure of 2-hydroxy benzo[a]carbazole-3-carboxylate (BCZC).

2. Experimental section

Materials

2-Hydroxy benzo[a]carbazole-3-carboxylate sodium (BCZC) was purchased from Sigma Chemical Co. Ltd. NaOH (AR), $Mg(NO_3)_2 \cdot 6H_2O$ (AR) and Al $(NO_3)_3 \cdot 9H_2O$ (AR) were purchased from Beijing Chemical Co. Ltd and used without further purification. All the aqueous solutions were prepared with deionized and CO_2-free water.

Preparation of BCZC intercalated Mg–Al-LDH

BCZC intercalated Mg–Al-LDH was prepared by the co-precipitation method. The matched molar ratios of Mg^{2+}/Al^{3+}/OH^-/BCZC were 2.0 : 1.0 : 6.0 : 1.0 or 3.0 : 1.0 : 8.0 : 1.0. Typically, 100 ml of a solution containing 5 mmol (or 7.5 mmol) $Mg(NO_3)_2 \cdot 6H_2O$ and 2.5 mmol $Al(NO_3)_3 \cdot 9H_2O$ was slowly added dropwise to 100 ml of a mixture solution (deionized water/glycol 1 : 1, v/v) containing 15 mmol (or 20 mmol) NaOH and 2.5 mmol BCZC with vigorous agitation under a nitrogen flow. The pH value at the end of addition was adjusted to 8.0 by further addition of 2.4 mol L^{-1} NaOH solution. The reaction mixture was subsequently heated at 70 °C for 24 h, washed thoroughly with deionized water and dried at 70 °C for 20 h. Based on the results of elemental analysis (Mg 8.63%, Al 5.39%, C 40.75%, N 1.90%, and H 4.09% for Sample A; Mg 12.34%, Al 4.43%, C 33.47%, N 2.79%, and H 4.45% for Sample B), the chemical composition of BCZC/Mg–Al-LDH can be determined as: $Mg_{1.929}Al_{1.071}(OH)_6(C_{17}H_9NO_3)_{1.071} \cdot 3.14H_2O$ (Sample A; Mg/Al ratio = 1.801) or $Mg_{2.274}Al_{0.726}(OH)_6(C_{17}H_9NO_3)_{0.726} \cdot 3.58H_2O$ (Sample B; Mg/Al ratio = 3.132). It should be noted that the water content was determined by TG-DTA analysis with the assumption that the interlayer water molecules are totally evaporated before 190 °C. The LDH films were prepared by the solvent evaporation method. Typically, an ethanol suspension of BCZC/LDH (1 mg mL^{-1}) was thoroughly dispersed under ultrasonication and then placed on a quartz substrate that was fully cleaned with anhydrous ethanol.

Characterization

The samples of BCZC/Mg–Al-LDH (Sample A and Sample B) were characterized on a Rigaku D/MAX2500VB2+/PC X-ray diffractometer, using Cu-Kα radiation (0.154184 nm) at 40 kV, 30 mA with a scanning rate of 5°/min, a step size of 0.02°/s, and a 2θ angle ranging from 3 to 70°. The Fourier transform infrared (FT-IR) spectra were recorded using a Nicolet 605 XB FT-IR spectrometer in the range 4000–400 cm^{-1} with 4 cm^{-1} resolution under air. The standard KBr disk method (1 mg of sample in 100 mg of KBr) was used. The solution and solid UV-vis absorption spectra were collected in the range 200–800 nm on a Shimadzu U-3000 spectrophotometer, with the slit width of 1.0 nm and $BaSO_4$ as the reference. The solution and solid state fluorescence spectra were performed on a RF-5301PC fluorospectrophotometer with an excitation wavelength of 410 nm. The width of both the excitation and emission slits is 3 nm. TG-DTA was measured on a PCT-1A thermal analysis system under ambient atmosphere with a heating rate of 10 °C min^{-1}. Analysis of metal contents was performed by ICP atomic emission spectroscopy on a

15086 | *Phys. Chem. Chem. Phys.*, 2010, **12**, 15085–15092

This journal is © the Owner Societies 2010

Shimadzu ICPS-7500 instrument using solutions prepared by dissolving the samples in dilute nitric acid. Carbon, hydrogen and nitrogen analyses were carried out using a Perkin Elmer Elementarvario elemental analysis instrument.

3. Structure model and simulation method

Two models of a $6 \times 3 \times 1$ Mg–Al-LDH rhombohedral supercell with $R\bar{3}m$ space group were constructed based on the rule that Al atoms will not occupy adjacent octahedra, and the details were fully described in our previous work.[7m,n] The LDH layer contains 12 Mg atoms and 6 Al atoms (Mg/Al ratio of 2, shown in Fig. 1A), and the other one contains 14 Mg atoms and 4 Al atoms (Mg/Al ratio of 3.5, shown in Fig. 1B). It is known that both of the two LDH layer models with different charge densities are close to the experimental ones. Therefore, every octahedra layer has 18 metal atoms and 36 OH groups. The distance between adjacent metal atoms is 3.05 Å, in accordance with the literature[7] and our experimental results below. A supercell was constructed based on the model of host layer, with lattice parameters $a = 18.30$ Å, $b = 9.15$ Å, $c = 24.0$ Å (experimental result), $\alpha = \gamma = 90°$, $\beta = 120°$. The supercell was treated as $P1$ symmetry and all lattice parameters were considered as independent variables in the simulation. A 3D periodic boundary condition[9] was applied in the system, and the simulated supercell can be repeated infinitely in three directions. To maintain electrical neutrality over the whole system, six and four BCZC anions (shown in Fig. 1C) were introduced into the simulated supercell with Mg/Al ratios of 2 and 3.5, respectively, with the perpendicular configuration respecting to the layer as an initial state. Furthermore, according to the experimental result, 16 and 20 water molecules were located in the two supercells with Mg/Al ratios of 2 and 3.5 randomly, based on the assumption that these molecules occupy the whole available interlayer space as much as possible. As a result, the formulae of the two simulated structures can be expressed as: $Mg_{12}Al_6(OH)_{36}(C_{17}H_{10}NO_3)_6 \cdot 16H_2O$ (named as model A), and $Mg_{14}Al_4(OH)_{36}(C_{17}H_{10}NO_3)_4 \cdot 20H_2O$ (named as model B).

A modified cff91 forcefield was employed to perform MD simulation in the whole process. A charge equilibration (QEq) method[10] was used to calculate atomic charges of the layer, in which the partial charges are +0.703e for Mg, +1.363e for Al, −0.537e for O and +0.243e for H in model A, and +0.695e for Mg, +1.355e for Al, −0.545e for O and +0.235e for H in model B. Other forcefield parameters for the anions and water molecules were also referred to the cff91 forcefield.[11] The NBO
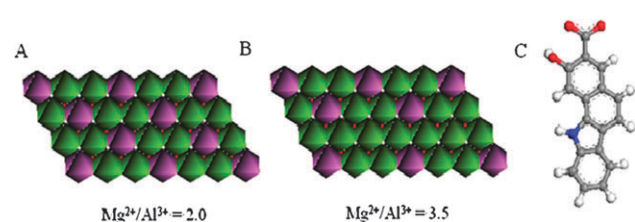
analysis[12] was employed to calculate the partial charges of BCZC anion at the B3LYP/6-31G** level using the Gaussian 03 programs.[13] For water molecules, the partial charges came from the simple point charge (SPC) water model reported by Berendsen.[14] In potential energy calculations, the long range coulomb interactions between partial charges were computed by the Ewald summation technique[9] and a "spline cutoff" method was used to calculate van der Waals interactions. After energy minimization was applied to the initial model, MD simulations were performed in an isothermal–isobaric (NPT) ensemble with a temperature of 300 K and a pressure of 0.1 MPa (about 1 atm). The Andersen method[15] and Berendsen method[16] were used to regulate the temperature and pressure, respectively. The total simulation time was 200 ps with a simulation time step of 1 fs. The result shows that the system reaches equilibrium with lattice parameters and total potential energy fluctuating around a constant value within the first 20 ps, as a result the dynamic trajectories were recorded every 20 fs in the remaining 180 ps in order to analyze the ensemble average values. All the simulations were performed using the Discover module in the Material Studio software package.[17]

4. Results and discussion

4.1 Experimental section

A Structural characterization of BCZC intercalated Mg–Al-LDH. The powder XRD pattern of BCZC/Mg–Al-LDH (Sample A) is shown in Fig. 2a. In this case, all the reflections can be indexed to a rhombohedral lattice with $R\bar{3}m$ symmetry, which is commonly used for the description of 3R-type LDH structure. The main characteristic reflections of Sample A appear at 3.69° (d_{003} = 2.392 nm), 7.79° (d_{006} = 1.134 nm), 11.62° (d_{009} = 0.761 nm), 15.49° (d_{0012} = 0.572 nm), 19.49° (d_{0015} = 0.455 nm), 22.93° (d_{0018} = 0.387 nm), and 61.30° (d_{110} = 0.304 nm). It was found that d_{003} (2.392 nm), d_{006} (1.134 nm) and d_{009} (0.761 nm) present a good multiple relationship for the basal, second- and third-order reflections. The lattice parameter c can be calculated from averaging the positions of the three harmonics: $c = 1/3 (d_{003} + 2d_{006} + 3d_{009}) = 2.314$ nm, which is related to several factors (such as the arrangement of interlayer anions, van der Waals radii of BCZC and the hydration state). For the sample
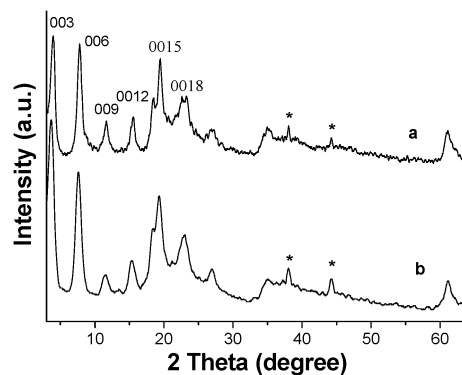

Fig. 1 The $6 \times 3 \times 1$ superlattice layer model for Mg–Al-LDH (color codes: dark pink: $Al(OH)_6$ octahedra; green: $Mg(OH)_6$ octahedra) for (A) Mg/Al ratio of 2; (B) Mg/Al ratio of 3.5; (C) structural model of 2-hydroxy benzo[a]carbazole-3-carboxylate (BCZC).

Fig. 2 Powder XRD patterns of BCZC /Mg–Al-LDH (a, b stand for Samples A and B, respectively). *: the Al substrate.

This journal is © the Owner Societies 2010

Phys. Chem. Chem. Phys., 2010, **12**, 15085–15092 | 15087

of BCZC/Mg–Al-LDH (Sample B, Fig. 2b), the crystallinity was similar to that of Sample A. The basal and second reflections were observed at 3.65° (2.418 nm) and 7.46° (1.185 nm), and the basal spacing is 2.394 nm. The lattice parameter a, which stands for the shortest distance of adjacent metal atoms with identical chemical environment in the LDH layer, can be calculated using: $a = 2d_{110}$. The values of a for the two samples are 3.03 (Sample A) and 3.04 Å (Sample B), in accordance with other reported MgAl-LDH systems (3.04 or 3.05 Å).[8] The values of a and c are referenced in the computer simulation section.

Fig. 3 shows the FT-IR spectra of pristine BCZC and the BCZC/LDH samples. The IR bands are assigned based on the literature.[7m,n,18] For pristine BCZC, the bands at 3425 and 1421 cm^{-1} are attributed to the stretching and in-plane deformation vibrations of O–H. The one at 3038 cm^{-1} corresponds to the =C–H stretching vibration within phenyl rings. Two bands assigned to the vibrations of C=O in –COO$^-$ groups appear at 1657 and 1623 cm^{-1}, and the bands at 1595 and 1562 cm^{-1} due to the skeleton vibration of phenyl rings can also be observed. The in-plane bending vibrations of =C–H in phenyl rings are located at 1224 and 1016 cm^{-1}. When the BCZC anion was intercalated into the Mg–Al-LDH layer (Mg/Al ratio = 1.801) (Fig. 3b), only one band was resolved as the vibration of C=O, with a red shift from 1657 to 1647 cm^{-1} ($\Delta = -10$ cm^{-1}), indicating the strong interactions between the carboxylate group and Mg–Al-LDH layers. The bands at 1598 and 1550 cm^{-1} are assigned to the stretching vibrations of phenyl rings. The FT-IR spectrum of BCZC/Mg–Al-LDH (Sample B) is displayed in Fig. 3c. The vibrations of C=O of –COO$^-$ moved to 1637 ($\Delta = -20$ cm^{-1}) and 1617 cm^{-1} ($\Delta = -6$ cm^{-1}), compared with those of pristine BCZC. The lattice vibration of the inorganic LDH layers appears in the range from 400 to 800 cm^{-1}. Moreover, the vibration bands owing to BCZC become weak and broad upon intercalation into the LDH layer, indicating that the rigid framework of LDH suppresses the vibration of the BCZC backbone due to the electrostatic and/or van der Waals interactions.
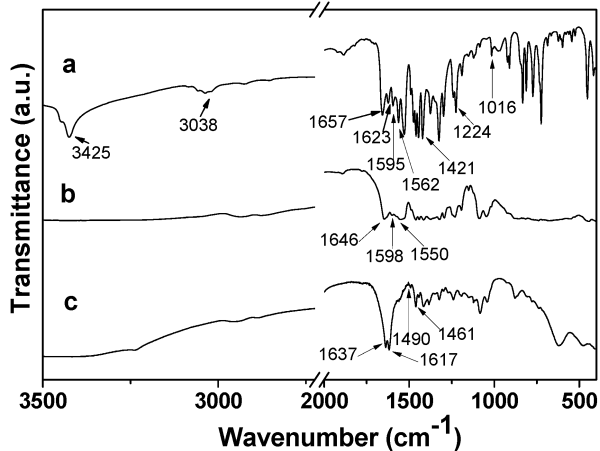
B Thermal decomposition of BCZC/Mg–Al-LDH.

The thermolysis behavior of pristine BCZC was studied firstly, and its TG-DTA curves are displayed in Fig. 4a. It was found that no obvious thermolysis can be observed until the temperature increases to ca. 300 °C. The sharp mass loss (315–600 °C) with the exothermic peak at 328 °C in the DTA curve is attributed to the decomposition and combustion of BCZC. In the case of BCZC/Mg–Al-LDH (Sample A, Fig. 4b), the thermal decomposition process can be characterized by three mass loss steps. The first one from room temperature to 190 °C (with the mass loss of 10.41%) is due to the removal of surface adsorbed and interlayer water
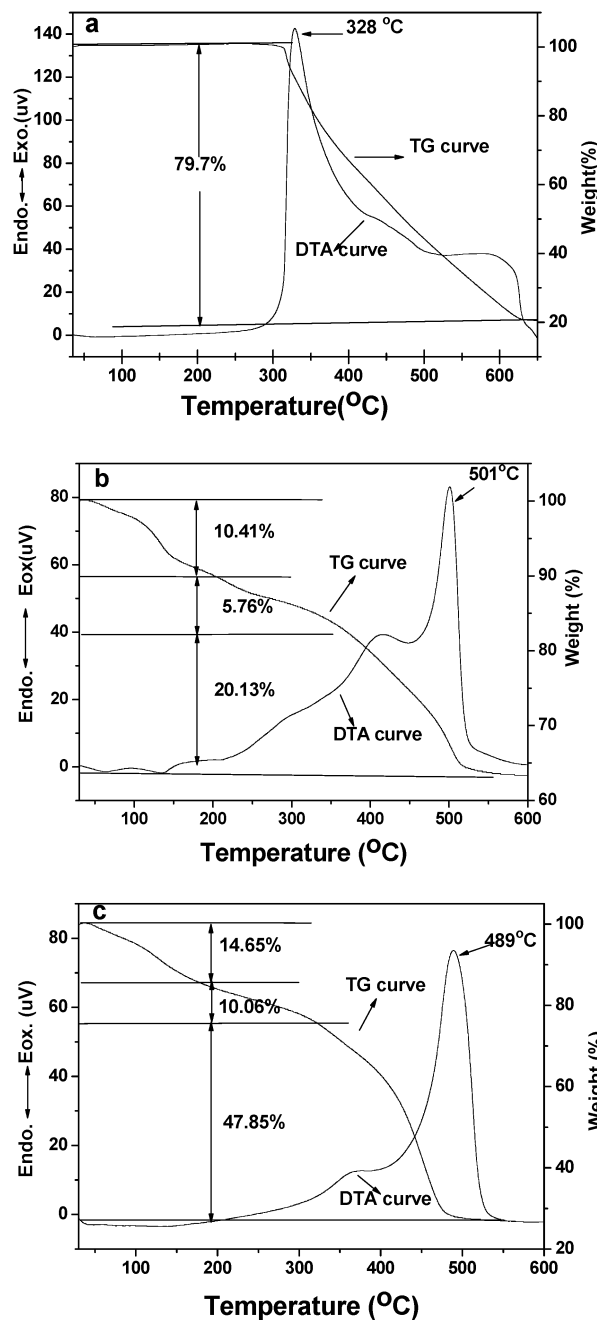

Fig. 3 FT-IR spectra for (a) BCZC, (b) BCZC/Mg–Al-LDH (Sample A) and (c) BCZC/Mg–Al-LDH (Sample B).

Fig. 4 TG and DTA curves for (a) pristine BCZC, (b) BCZC/Mg–Al-LDH (Sample A), (c) BCZC/Mg–Al-LDH (Sample B).

molecules.[4] The second one with a gradual mass loss of 5.76% in the temperature range 190–350 °C mainly derives from the decomposition and dehydroxylation of the brucite-like layers.[19] The third one corresponds to the decomposition or combustion of BCZC and collapse of the layer, accompanied by a strong exothermic peak at *ca.* 501 °C in the DTA curve.[5b,7o] Fig. 4c shows the TG-DTA curves of Sample B. It can be observed that the three mass losses of 14.65%, 10.06% and 47.85% occur in the temperature ranges 30–190 °C, 190–350 °C and 350–600 °C, respectively. Moreover, the strong exothermic peak corresponding to the combustion of BCZC appears at 489 °C, a little lower than that of Sample A. Therefore, it can be concluded that the combustion temperature of BCZC increases largely by *ca.* 160 °C upon intercalation into the LDH gallery, and this can be attributed to the host–guest interactions (including coulombic, hydrogen interactions, and so on) between the carbazole anions and LDH layer.[5b]

C Photophysical properties of BCZC/Mg–Al-LDH.
Fig. 5A(a) shows the UV-vis absorption spectrum of the pristine BCZC aqueous solution (10 μM). The absorption bands observed at 265, 289 and 320 nm are attributed to the characteristic absorptions of carbazole-type dyes. For the solid BCZC sample (Fig. 5A, curve b), the absorption is integrated into a broad band around 295 nm; moreover, a strong band is resolved at 410 nm, which can be attributed to the molecular
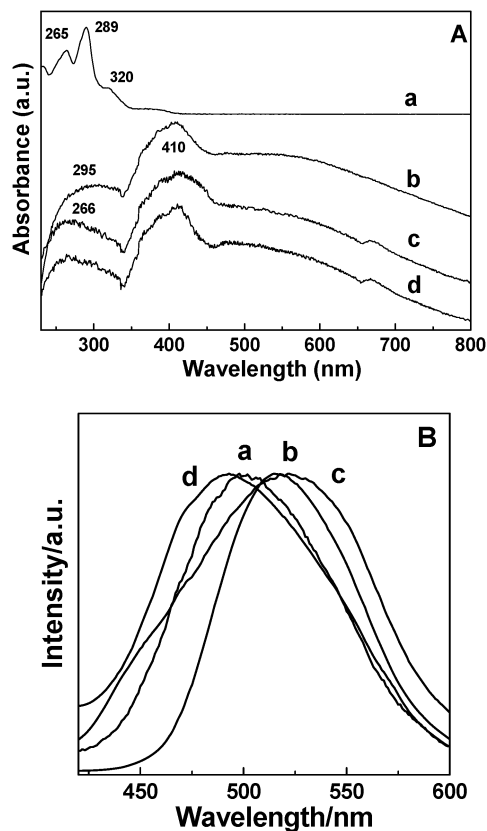

Fig. 5 (A) The UV-vis absorption spectra and (B) normalized photoemission spectra for (a) pristine BCZC aqueous solution (10 μM), (b) solid BCZC, (c) BCZC/Mg–Al-LDH (Sample A), and (d) BCZC/Mg–Al-LDH (Sample B).

stacking of BCZC in its solid state.[5b] The UV-vis absorption spectra for BCZC/Mg–Al-LDHs with different LCDs are shown in Fig. 5A(c) and A(d). Both of their absorption bands appear at 266 and 410 nm, similar to that of the pristine solid BCZC.

The fluorescence emission spectra for the BCZC aqueous solution (10 μM), its solid sample and BCZC/Mg–Al-LDH samples are displayed in Fig. 5B(a)–(d). The symmetrical emission peak can be observed at 499 (Fig. 5B(a)) and 517 nm (Fig. 5B(b)) with the FWHM of *ca.* 90 and 78 nm for the BCZC aqueous solution and its solid state, respectively. The red-shift for the BCZC solid sample can be attributed to the π–π or dipole–dipole interaction of the conjugated BCZC molecule. Moreover, the relatively broad emission peaks of Sample A and Sample B were observed at 522 and 494 nm with the FWHM of *ca.* 111 and 104 nm, respectively (Fig. 5B(c, d)). Therefore, it can be concluded that the photoemission behavior of the interlayer BCZC is close to that of its solid state and aqueous solution state between the LDH layer with Mg/Al ratios of 1.801 and 3.132, respectively. Meanwhile, these results suggest that the luminescence performance of the dye molecules can be tuned by adjusting the LCD of LDH.

D The characterization of BCZC/Mg–Al-LDH thin film.
Fig. 6 show the XRD patterns of BCZC/Mg–Al-LDH (Sample A and B) thin films. The strong basal reflections (00*l*) and the absences of any non-basal reflections (*h, k* ≠ 0) for the BCZC/Mg–Al-LDH thin films can be observed, compared with the corresponding powder samples, illustrating the extremely good *c*-oriented assembly of LDH platelets (*ab* plane of LDH platelets parallel to the substrates). To further investigate the preferred orientation and polarized fluorescence properties of the as-prepared BCZC/Mg–Al-LDH powder and thin film samples, the anisotropic value *r* was determined.[20] *r* can be expressed as the formula:

$$r = \frac{I_{VV} - GI_{VH}}{I_{VV} + 2GI_{VH}} \quad (1)$$

where $G = \frac{I_{HV}}{I_{HH}}$; I_{VH} stands for the photoluminescence intensity obtained with vertical polarized light excitation and horizontal polarization detection, and I_{VV}, I_{HH}, I_{HV} are defined in a similar way. Theoretically, the *r* value is in the range from
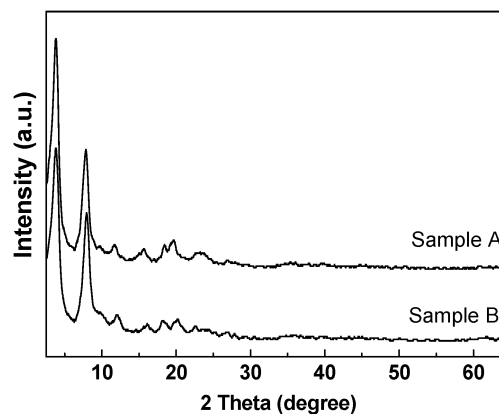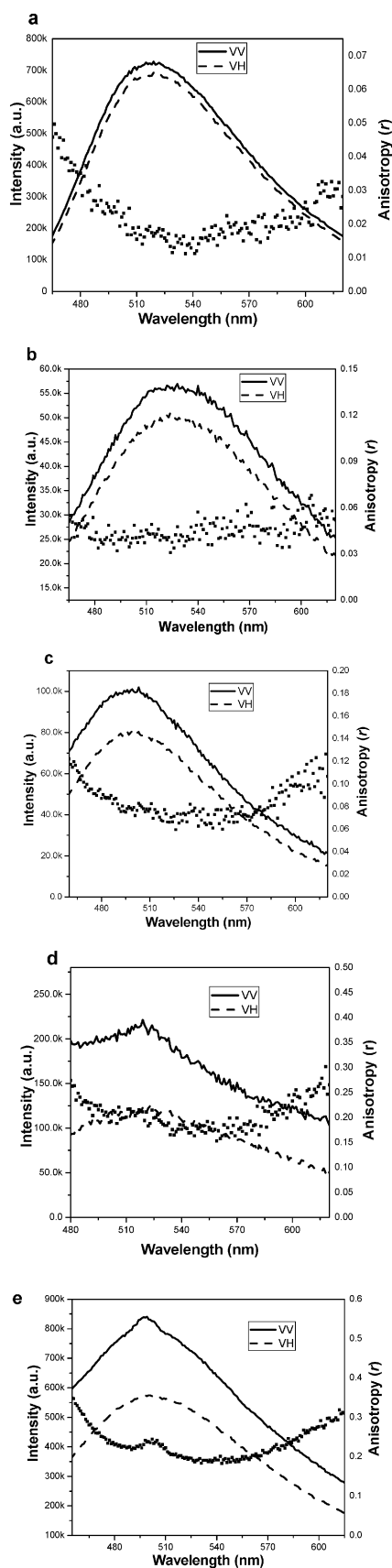

Fig. 6 XRD patterns of BCZC/Mg–Al-LDH (Sample A and B) thin films.

−0.2 (absorption and emission transition dipoles are perpendicular) to 0.4 (two transition dipoles are parallel).

For the pristine BCZC solid sample, the average r value was found to be 0.017 in the range 500–550 nm, indicating its isotropy. However, the average r values are 0.043 for Sample A in the range 500–540 nm (Fig. 7b) and 0.076 for Sample B in the range 490–520 nm (Fig. 7c), with an enhancement of *ca.* 2.5–5.8 times upon intercalation of BCZC. This indicates the ordered arrangement of the guest anions in the LDH gallery. The average r value of Sample B is higher than that of Sample A, suggesting a more preferred arrangement of BCZC in the layer with Mg/Al ratio of 3.132. Moreover, the polarized photoemission spectra and corresponding r values of BCZC/Mg–Al-LDH thin films are displayed in Fig. 7d and e, from which it can be found that the r values are further enhanced (*ca.* 0.15–0.2) compared with the powder samples, confirming that the dye/LDH thin film exhibits a well-oriented and uniformly ordered structure, in good agreement with the XRD observations. The value of r less than 0.4 can be attributed to the following reasons: (1) the absorption and emission transition dipole moments are not absolutely parallel; (2) there is a distribution of orientations of the carbazole anions; (3) the carbazole anions undergo slow rotational motion and diffusion in the gallery of LDH. This will be further discussed in the MD simulation section.

4.2 Molecular dynamics simulation

A The basal spacing and structures of guest anions between the LDHs layers. The simulated basal spacings are 23.70 and 23.74 Å for models A and B respectively, consistent with the experimental ones (23.14 and 23.94 Å), demonstrating the validity of MD simulation for this dye/LDH system. The interlayer arrangement and orientation of the guest molecules provide key information for understanding the host–guest structures and interactions. In this section, the orientation angle of BCZC with respect to the LDH layer was defined so as to describe the geometries of guest molecules (shown in the inset of Fig. 8). For the BCZC/Mg–Al-LDH (Model A), the orientation angle (θ) is mainly populated from 15 to 51° with
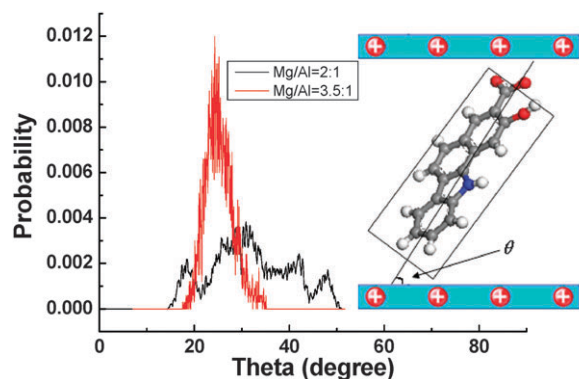
Fig. 8 The distributions of orientational angle θ (the plane of BCZC with respect to the LDH layer) with different LCDs of the LDH layer.

Fig. 7 Photoemission profiles in the VV, VH polarizations and anisotropic value (r) measured at room temperature (293 K) for: (a) the pristine BCZC powder, (b) powder state of Sample A, (c) powder state of Sample B, (d) thin film of Sample A, (e) thin film of Sample B.

15090 | *Phys. Chem. Chem. Phys.,* 2010, **12**, 15085–15092

This journal is © the Owner Societies 2010

the optimal angle at 31°, whereas it exhibits a nearly normal distribution in the range from 19 to 35° with the optimal angle at 24° for BCZC/Mg–Al-LDH (Model B). Therefore, the BCZC anions are more likely inclined to the Mg–Al-LDH layers in Model B than those in Model A. Moreover, the distribution of BCZC anions is much broader in Model A than that in Model B, suggesting that BCZC anions are accommodated in the LDH gallery in a more orderly fashion in Model B. This result is responsible for the larger luminescent anisotropic value for BCZC/Mg–Al-LDH (Sample B) than that of BCZC/Mg–Al-LDH (Sample A).

Fig. 9 shows MD simulation snapshots of the BCZC anion intercalated Mg–Al-LDH with two different LCDs of the LDH layer, which can help to further understand the structure and orientation of BCZC anions in the gallery of Mg–Al-LDH. It can be observed that the BCZC anions were arranged close together between the Mg–Al-LDH layers (Model A, Fig. 9A), whereas they exhibit a nearly bilayer arrangement in Model B (Fig. 9B). For BCZC/Mg–Al-LDH (Model A), the van der Waals volumes of BCZC overlap each other, which gives rise to the π–π or dipole–dipole interaction of dye anions. This is a reasonable explanation for the red shift behavior of the luminescence of BCZC/Mg–Al-LDH (Sample A). In contrast, the separation of adjacent BCZC anions was increased because of the low LCD in Model B, accounting for the absence of aggregation of BCZC. Moreover, the conjugated carbazole groups of BCZC are inclined to stack in the intermediate position of the LDH gallery, which corresponds to the hydrophobic and nonpolar environment, whereas the carboxylate groups mainly occupy the hydrophilic and polar region close to the LDH layers.

The behavior of calculated mean square displacements (MSD) vs. simulation time for the intercalated BCZC anions is shown in Fig. S1 in the ESI†. The diffusion coefficients of BCZC are 0.82×10^{-10} (Model A) and 1.06×10^{-10} m^2 s^{-1} (Model B), illustrating that the diffusion resistance of BCZC in Model A layers is higher than that in Model B. This can be attributed to the relatively closer stacking of BCZC anions in Model A.[7b]

The radial distribution functions (RDF) of O–O and O–H for interlayer water molecules were also simulated for probing the properties of the confined water. For the O–O RDF of water (Fig. S2a and S2b in the ESI†), the sharp peaks (2.85 and 2.87 Å) and the weak peaks (6.11 and 5.91 Å) correspond to the first and second coordination shell for Model A and Model B, respectively. The height of the first O–O peak in the range 6.6–7 Å, was ca. 3 times larger than that of bulk water (2.6–3.0 Å).[21] For the O–H RDF of water

(Fig. S2c and S2d in the ESI†), two sharp peaks with nearly the same intensity can be observed at ca. 1.90 and 3.24 Å. The first one can be attributed to the H bond interaction between the O atoms and their neighboring H atoms. The positions of the two peaks are very close to those of bulk water. Fig. S2e and S2f in the ESI† present the H–H RDF of interlayer water for the LDH layer (Mg/Al ratio of 2 and 3.5), for which two peaks at ca. 2.60 Å and 3.70 Å were observed. Moreover, the peak intensities for both the O–H and H–H RDF are larger than that of bulk water in terms of experimental and simulated results,[21] suggesting that the arrangement degree of interlayer water is largely improved compared with that of bulk water.

Conclusions

In summary, the photoluminescence and thermolysis properties of BCZC anion intercalated Mg–Al-LDH for both powder and thin film samples have been investigated. An important insight from this work is that the emission wavelengths (522 and 494 nm) of the guest dye are totally different in the LDH layer with two LCDs (Mg/Al = 1.801 and 3.132), suggesting that the luminescent properties can be adjusted and controlled by regulating the properties of the host LDH layer.

This feature may not be achieved by other cationic clay materials, showing that the LDHs have emerged as new materials in the field of luminescent applications. The combustion temperature of the dye anions is improved by at least 160 °C upon intercalation, demonstrating that the thermal stability of BCZC molecule is largely enhanced when in the gallery of LDHs. The polarized photoemission measurements show that the macroscopic anisotropy of the BCZC/Mg–Al-LDH films is improved significantly compared with the powder sample and the pristine BCZC, suggesting the uniform and ordered assembly of BCZC can be achieved in the LDH gallery. Molecules dynamics simulation shows that the BCZC anions are more likely inclined to the Mg–Al-LDH (Mg/Al = 3.5) layers, compared with the Mg–Al-LDH (Mg/Al = 2) layers. Additionally, the orientational distribution of BCZC anions is broader in Model A (Mg/Al = 2) than that in Model B (Mg/Al = 3.5), demonstrating that the arrangement of BCZC anions is more orderly in Model B, in agreement with experimental observation. The separation of dye molecules was increased for the Model B system, which suppressed the aggregation of dye. Moreover, the diffusion coefficient of BCZC in Model A is lower than that in Model B. The radial distribution functions for O–O, O–H, and H–H of the interlayer water were also investigated, which showed that the water is distributed in a more orderly fashion than in the bulk. Therefore, by virtue of combination of experimental technique and theoretical calculation, this work not only gives a detailed investigation into the photophysical properties and thermolysis of dye molecules confined in the LDH matrix, but also provides further understanding of the orientations, ordered arrangement and diffusion properties of the guest molecules in the gallery of LDH. It can be expected that BCZC/Mg–Al-LDH films may have potential applications in the field of polarized luminescence materials.
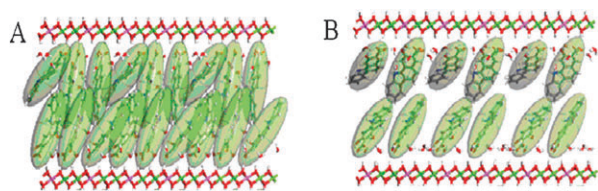

Fig. 9 Snapshots of the simulation for BCZC intercalated Mg–Al-LDH of (A) Model A and (B) Model B. The van der Waals volume of the interlayer BCZC anion is depicted in green.

This journal is © the Owner Societies 2010

Phys. Chem. Chem. Phys., 2010, **12**, 15085–15092 | 15091

Notes and references

1 C. M. Carbonaro, A. Anedda, S. Grandi and A. J. Magistris, *J. Phys. Chem. B*, 2006, **110**, 12932.

2 (a) B. Sels, D. De Vos, M. Buntinx, F. Pierard, K. D. Mesmaeker and P. Jacobs, *Nature*, 1999, **400**, 855; (b) B. M. Choudary, Ch. Venkat Reddy, B. V. Prakash, M. L. Kantam and B. Sreedhar, *Chem. Commun.*, 2003, 754.

3 (a) A. M. Fogg, V. M. Green, H. G. Harvey and D. O'Hare, *Adv. Mater.*, 1999, **11**, 1466; (b) A. I. Khan and D. O'Hare, *J. Mater. Chem.*, 2002, **12**, 3191.

4 Q. Yuan, M. Wei, D. G. Evans and X. Duan, *J. Phys. Chem. B*, 2004, **108**, 12381.

5 (a) U. Costantino, N. Coletti, M. Nocchetti, G. G. Aloisi, F. Elisei and L. Latterini, *Langmuir*, 2000, **16**, 10351; (b) D. P. Yan, J. Lu, M. Wei, D. G. Evans and X. Duan, *J. Phys. Chem. B*, 2009, **113**, 1381; (c) S. Gago, T. Costa, J. S. de Melo, I. S. Gonçalves and M. Pillinger, *J. Mater. Chem.*, 2008, **18**, 894; (d) L. Mohanambe and S. Vasudevan, *J. Phys. Chem. B*, 2006, **110**, 14345; (e) J. Bauer, P. Behrens, M. Speckbacher and H. Langhals, *Adv. Funct. Mater.*, 2003, **13**, 241; (f) D. P. Yan, J. Lu, M. Wei, J. B. Han, J. Ma, F. Li, D. G. Evans and X. Duan, *Angew. Chem., Int. Ed.*, 2009, **48**, 3073; (g) D. P. Yan, J. Lu, M. Wei, J. Ma, X. R. Wang, D. G. Evans and X. Duan, *Langmuir*, 2010, **26**, 7007; (h) D. P. Yan, J. Lu, M. Wei, J. B. J. Ma, D. G. Evans and X. Duan, *Chem. Commun.*, 2009, 6358.

6 (a) C. M. Carbonaro, A. Anedda, S. Grandi and A. Magistris, *J. Phys. Chem. B*, 2006, **110**, 12932; (b) I. García-Moreno, A. Costela, A. Cuesta, O. García, D. del Agua and R. Sastre, *J. Phys. Chem. B*, 2005, **109**, 21618.

7 (a) H. C. Greenwell, W. Jones, V. C. Peter and S. Stackhouse, *J. Mater. Chem.*, 2006, **16**, 708; (b) S. P. Newman, S. J. Williams, P. V. Coveney and W. Jones, *J. Phys. Chem. B*, 1998, **102**, 6710; (c) J. W. Wang, A. G. Kalinichev, R. J. Kirkpatrick and X. Q. Hou, *Chem. Mater.*, 2001, **13**, 145; (d) A. G. Kalinichev and R. J. Kirkpatrick, *Chem. Mater.*, 2002, **14**, 3539; (e) R. T. Cygan, J. J. Liang and A. G. Kalinichev, *J. Phys. Chem. B*, 2004, **108**, 1255; (f) H. Li, J. Ma, D. G. Evans, T. Zhou, F. Li and X. Duan, *Chem. Mater.*, 2006, **18**, 4405; (g) N. Kim, A. Harale, T. T. Tsotsis and M. Sahimi, *J. Chem. Phys.*, 2007, **127**, 224701; (h) J. Pisson, J. P. Morel, N. Morel-Desrosiers, C. Taviot-Guého and P. Malfreyt, *J. Phys. Chem. B*, 2008, **112**, 7856; (i) L. Mohanambe and S. Vasudevan, *J. Phys. Chem. B*, 2005, **109**, 15651; (j) M. M.-A. Thyveetil, P. V. Coveney, H. C. Greenwell and J. L. Suter, *J. Am. Chem. Soc.*, 2008, **130**, 4742; (k) P. P. Kumar, A. G. Kalinichev and R. J. Kirkpatrick, *J. Phys. Chem. B*, 2006, **110**, 3841; (l) H. Zhang, Z. P. Xu, G. Q. Lu and S. C. Smith, *J. Phys. Chem. C*, 2009, **113**, 559; (m) D. P. Yan, J. Lu, M. Wei, H. Li, J. Ma, F. Li, D. G. Evans and X. Duan, *J. Phys. Chem. A*, 2008, **112**, 7671; (n) D. P. Yan, J. Lu, M. Wei, J. Ma, D. G. Evans and X. Duan, *Phys. Chem. Chem. Phys.*, 2009, **11**, 9200; (o) D. P. Yan, J. Lu, J. Ma, M. Wei, S. H. Qin, L. Chen, D. G. Evans and X. Duan, *J. Mater. Chem.*, 2010, **20**, 5016; (p) D. P. Yan, J. Lu, L. Chen, S. H. Qin, J. Ma, M. Wei, D. G. Evans and X. Duan, *Chem. Commun.*, 2010, **46**, 5912.

8 (a) M. Bellotto, B. Rebours, O. Clause, J. Lynch, D. Bazin and E. Elkaim, *J. Phys. Chem.*, 1996, **100**, 8527; (b) Y. Zhao, F. Li, R. Zhang, D. G. Evans and X. Duan, *Chem. Mater.*, 2002, **14**, 4286.

9 (a) M. P. Allen and D. J. Tildesley, *Computer Simulation of Liquids*, Clarendon, Oxford, 1987; (b) A. R. Leach, *Molecular Modeling, Principles and Applications*, Pearson Education Ltd., England, 2nd edn, 2001; (c) S. Choi, J. Coronas, E. Jordan, W. Oh, S. Nair, F. Onorato, D. F. Shantz and M. Tsapatsis, *Angew. Chem., Int. Ed.*, 2008, **47**, 552.

10 A. K. Rappé and W. A. Goddard, *J. Phys. Chem.*, 1991, **95**, 3358.

11 J. R. Maple, M.-J. Hwang, T. P. Stockfisch, U. Dinur, M. Waldman, C. S. Ewig and A. T. Hagler, *J. Comput. Chem.*, 1994, **15**, 162.

12 A. E. Reed, L. A. Curtiss and F. Weinhold, *Chem. Rev.*, 1988, **88**, 899.

13 M. J. Frisch, G. W. Trucks, H. B. Schlegel, G. E. Scuseria, M. A. Robb, J. R. Cheeseman, J. A. Montgomery, Jr., T. Vreven, K. N. Kudin, J. C. Burant, J. M. Millam, S. S. Iyengar, J. Tomasi, V. Barone, B. Mennucci, M. Cossi, G. Scalmani, N. Rega, G. A. Petersson, H. Nakatsuji, M. Hada, M. Ehara, K. Toyota, R. Fukuda, J. Hasegawa, M. Ishida, T. Nakajima, Y. Honda, O. Kitao, H. Nakai, M. Klene, X. Li, J. E. Knox, H. P. Hratchian, J. B. Cross, C. Adamo, J. Jaramillo, R. Gomperts, R. E. Stratmann, O. Yazyev, A. J. Austin, R. Cammi, C. Pomelli, J. W. Ochterski, P. Y. Ayala, K. Morokuma, G. A. Voth, P. Salvador, J. J. Dannenberg, V. G. Zakrzewski, S. Dapprich, A. D. Daniels, M. C. Strain, O. Farkas, D. K. Malick, A. D. Rabuck, K. Raghavachari, J. B. Foresman, J. V. Ortiz, Cui, Q. A. G. Baboul, S. Clifford, J. Cioslowski, B. B. Stefanov, G. Liu, A. Liashenko, P. Piskorz, I. Komaromi, R. L. Martin, D. J. Fox, T. Keith, M. A. Al-Laham, C. Y. Peng, A. Nanayakkara, M. Challacombe, P. M. W. Gill, B. Johnson, W. Chen, M. W. Wong, C. Gonzalez and J. A. Pople, *GAUSSIAN 03 (Revision B.04)*, Gaussian, Inc., Pittsburgh, PA, 2003.

14 H. J. C. Berendsen, J. P. M. Postma, W. F. van Gunsteren and J. Hermans, *Interaction models for water in relation to protein hydration*, in *Intermolecular Forces*, ed. B. Pullman, Riedel, Dordrecht, The Netherlands, 1981, p. 331.

15 H. C. Andersen, *J. Chem. Phys.*, 1980, **72**, 2384.

16 H. J. C. Berendsen, J. P. M. Postma, A. van Gunsteren, A. DiNola and J. R. Haak, *J. Chem. Phys.*, 1984, **81**, 3684.

17 *Discover Module, MS Modeling*, Version 2.2, Accelrys Inc., San Diego, CA, 2003.

18 (a) H. Günzler and H. Gremlich, in *IR Spectroscopy: An Introduction*, Wiley-VCH, Verlag GmbH, 2002; (b) J. H. Lee, S. W. Rhee and D. Y. Jung, *Chem. Mater.*, 2004, **16**, 4774.

19 (a) C. Roland-Swanson, J.-P. Besse and F. Leroux, *Chem. Mater.*, 2004, **16**, 5512; (b) Q. Z. Yang, D. J. Sun, C. G. Zhang, X. J. Wang and W. A. Zhao, *Langmuir*, 2003, **19**, 5570.

20 B. Valeur, *Molecular Fluorescence: Principles and Applications*, Wiley-VCH, Verlag GmbH, 2001.

21 A. Wauqvist and B. J. Berne, *J. Phys. Chem.*, 1993, **97**, 13841.